ACS OMEGA

Open Access

http://pubs.acs.org/journal/acsodf

Article

Magnesium Oxychloride and Magnesium Oxysulfate Cements as Temporary Plugging Agents in Geothermal Drilling

Liangliang Yan, Shaocong Pang, Haiyan Dong, Xiuhua Zheng, and Yuxiu An*

Cite This: *ACS Omega* 2024, 9, 2696−2706

Read Online

ACCESS | Metrics & More | Article Recommendations

ABSTRACT: The development and utilization of geothermal resources are effective ways to alleviate the current haze situation, adjust the energy structure, and achieve energy conservation and emission reduction. Geothermal formations typically contain extensive fracture networks, with fracture openings. These fracture networks can result in substantial losses of the drilling fluid and increased costs for geothermal drilling. Temporary plugging cements are used to solve the problem of lost circulation due to their high strength and high acid solubility. In this paper, two types of temporary plugging materials, magnesium oxysulfate (MOS) cement and magnesium oxychloride (MOC) cement, were prepared. The influence of the plugging agent on the flow field and the force exerted on the solid under the action of the fluid was analyzed using fluid−solid coupling software. The simulation results show that when subjected to a flow rate of 10 m/s, the edge of the cement experiences a significant force, while the stress is not widely transmitted to the middle and rear of the cement. This indicates that the cement has a strong resistance to the fluid flow. The fundamental characteristics of MOC cement and MOS cement, such as compressive strength and setting time, were investigated. The test results show that adjusting the molar ratio of the two types of cements can shorten the setting time by 60% and increase the compressive strength to up to 23 MPa. In addition, the acid solubility of the cement with different ratios of raw materials is above 95%. The plugging performance of these two cements as loss circulation materials was evaluated by using a physical simulation device. The pressure bearing capacity of the MOC cement with different $MgO/MgCl_2{\cdot}6H_2O/H_2O$ molar ratios ranged between 13.4 and 23.6 MPa. The maximum bearing capacity of the MOS cement can reach up to 18.6 MPa. The results showed that both cements possess excellent plugging and pressure bearing capacity.

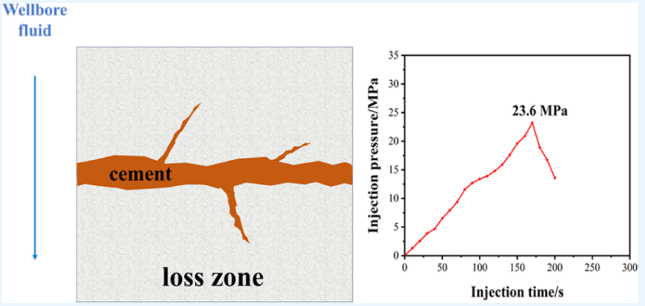

1. INTRODUCTION

As an important part of promising clean and renewable energy, geothermal energy is considered one of the most effective methods for reducing carbon emissions. With its abundant reserves and independence from climate and sunshine, geothermal energy has been garnering increasing attention from countries worldwide.[1] Geothermal reservoirs are often closely related to geological structures, which lead to highly developed fractures. Lost circulation is a serious problem during geothermal drilling.[2,3] From an economic perspective, the cost of drilling a geothermal well typically represents 30−50% of the overall geothermal project cost, while lost circulation accounts for 10−20% of the cost of drilling a geothermal well.[4,5] In addition, uncontrolled fluid loss can damage the reservoir and have a negative impact on its production capacity.[6,7] If losses continue to occur, it can lead to drilling accidents such as downhole sticking and even blowouts.[8] Under typical circumstances of fluid loss, conventional lost circulation materials (LCMs) (e.g., nutshell, calcium carbonate, resilient graphitic carbon (RCG), rubber) are commonly directly added to the drilling fluid. This helps mitigate partial losses to some degree.[9] The plugging materials of various sizes and shapes are mixed with the drilling fluid to bridge, accumulate, and fill in the cracks. This forms a layer of the plugging material that blocks the transmission of fluid pressure and the flow of fluid medium through the cracks..[10−12] However, in the case of severe or total losses, drilling should be halted immediately and plugging slurry, which consists of gunk, cement, and other materials, should be injected into the loss zones to enhance the pressure bearing capacity of the formation.[13] However, the defects of the mentioned LCMs are exposed in practical applications. The granular materials cannot form a stable blockage, and it may be cleared early in the event of large fluctuations in downhole

Received: October 4, 2023
Revised: December 10, 2023
Accepted: December 13, 2023
Published: December 29, 2023

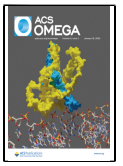

Table 1. Main Components of Light-Burned MgO

component	MgO	SiO_2	CaO	Al_2O_3	Fe_2O_3	ignition loss
content, %	86.15	5.47	1.59	0.37	0.30	6.12

pressure.[14−17] Moreover, while high concentrations and large-sized LCM mixtures can have a good bridging plugging effect, they may also plug the drill nozzle. Additionally, determining the exact size characteristics of the loss zones (e.g., pore size or crack width) is very challenging. Therefore, designing a suitable particle size distribution (PSD) of LCMs is difficult.[18] The polymer plugging material can form a versatile viscoelastic gel that can conform to different types of cracks. However, the compressive or tensile strength of the gel needs to be improved, which may flow out during the recovery drilling process, resulting in drilling fluid loss.[19,20] Inorganic cross-linked LCM (e.g., cement) is the main treatment method for major losses.[21,22] The success rate is relatively high, but the cost is also high. The cement waiting time is long and the acid solubility of the cement is low, which will cause significant damage to the reservoir. Therefore, the development of suitable plugging materials is crucial for controlling lost circulation and maximizing the utilization of geothermal resources.

To overcome the limitations of the above-mentioned materials, temporary plugging agents are widely used as a solution for loss treatment. This type of materials can be used in various ways to unblock formations at a later stage without causing any damage. According to the method of plug removal, the temporary plugging agent can be categorized into an acid-soluble temporary plugging agent, water-soluble temporary plugging material, and oil-soluble temporary plugging agent. Among these, acid-soluble temporary plugging agents (e.g., acid-soluble cements) are the most commonly used. Magnesium oxysulfate (MOS) cement (i.e., a mixture of magnesium oxides and magnesium sulfates) and magnesium oxychloride (MOC) cement (i.e., a mixture of magnesium oxides and magnesium chlorides) have attracted wide attention because of their advantages of rapid solidification, early strength, high strength, salt water corrosion resistance, and high acid solubility. Vinson et al. reported the MOC cement to be an acid-removable cement system to reduce severe losses in producing ones.[23] Mata, F et al. compared the difference between the MOC cement and traditional cement in plugging and concluded that the MOC cement should be prioritized in the loss of reservoir sections with excellent acid solubility.[24] However, only the acid solubility and plugging ability of the MOC cement were studied. Magnesium oxysulfate (MOS) cement has low hygroscopicity, making it easier to transport and giving it a longer shelf life.[25,26] Commonly, the strength of the MOS cement is lower due to the limited solubility of $MgSO_4·7H_2O$ at ambient temperature. However, this can be effectively improved by raising temperatures or by adding modifying additives.[27,28] Cui et al. studied the fundamental properties and plugging performance of the MOS cement. They successful applied it in the Junggar Basin, Xinjiang, China, and verified its significant plugging effect for severe loss problems.[29] However, there is a lack of systematic research on the setting time of MOS cement. In the present study, there is a lack of systematic testing of MOC cement and MOS cement as plugging materials, and there are few studies on these two cements as temporary plugging agents for geothermal drilling. Thus, in order to mitigate the loss of the drilling fluid and minimize damage to the reservoir in geothermal drilling, it is also essential to conduct a comprehensive study of the performance of MOC cement and MOS cement.

In this paper, we proposed using different molar ratios of raw materials for MOC cement and MOS cement. We evaluated their potential as temporary plugging agents in geothermal drilling through various experimental methods. In order to further explore the effect of the molar ratio of raw materials on the structure of cement, scanning electron microscopy (SEM) was performed. Studies have shown that both cements can provide a rapid and effective solution to geothermal well losses.

2. MATERIALS AND METHODS

2.1. Raw Materials. Light-burned magnesia powder (MgO, industrial reagent, purity ≥85%) was purchased from Yingkou Renxing Magnesium Industry Co., Ltd. (China). It had a mean particle size of 12.095 mm and a hydration activity of 64.11% (see Table 1 for details). Magnesium chloride hexahydrate ($MgCl_2·6H_2O$, purity ≥99%) was a white flake crystal, and magnesium sulfate heptahydrate ($MgSO_4·7H_2O$, purity ≥99%) was a colorless fine needle crystal, which was provided by Shouguang Jujiong Chemical Co., Ltd. (China).

2.2. MOC Cement and MOS Cement Slurry Preparation. The MOC cement slurry consisted of $MgCl_2·6H_2O$, MgO, and H_2O. The quality of raw materials was determined based on the molar ratio. Magnesium chloride was poured into deionized water and stirred until completely dissolved to form a solution. Then, the required amount of MgO powder was added and stirred for several minutes to make the MOC cement slurry. The MOS cement slurry consisted of $MgSO_4·7H_2O$, MgO, and H_2O. The preparation method of MOS cement is similar to that of MOC cement. However, because magnesium sulfate has low solubility in water, the solution must be heated and stirred until it is fully dissolved. Then, the required amount of MgO powder was poured and stirred for several minutes to create the MOS cement slurry.

2.3. Setting Time Measurement. The setting time of MOS cement and MOC cement slurries was determined using a Vicat apparatus. The tester was adjusted so that the test needle makes contacts with the glass plate pointer to the zero point. It is ensured that the test needle is adjusted to stop when it just touched the surface of the cement paste. After tightening the screw for 1−2 s, it suddenly loosens, allowing the test needle to sink freely into the cement paste vertically. The reading of the pointer was observed when the test needle stops sinking. When the initial setting test needle sinks to about 4 mm from the floor, it indicates that the cement has reached its initial setting state. The time it takes for the cement slurry to reach this state, from the moment the MgO powder is added, is referred to as the initial setting time of the cement. When the final setting test needle sinks into the test body by 0.5 mm and the annular attachment does not leave any marks on the test body, it indicates that the cement has reached its final setting state. The time taken from adding MgO powder to reaching the final setting state is referred to as the final setting time of the cement.

https://doi.org/10.1021/acsomega.3c07654
ACS Omega 2024, 9, 2696−2706

2.4. Compressive Strength Measurement and Microstructure Characterization. The cement slurry was poured into a mold measuring 5 cm × 5 cm × 5 cm and left to cure at room temperature for 24 h, resulting in the preparation of cement cube samples. The compressive strength of each sample was determined by calculating the average compressive strength of three cubes by using a uniaxial compression tester with a loading rate of 1 mm/s. After the compressive strength test was conducted, the fragments from the fracture surface were collected and transformed into samples of comparable size. Then, the sample was vacuumed, and gold plating was carried out. The microstructures were characterized under scanning electron microscopy (SEM) after gold coating.

2.5. Acid Solubility Test. The acid solubility experiment may be affected by a series of parameters (e.g., solidification time, sample size, acid type, acid concentration, and treatment time).[30] The acid used in this test was limited to HCl, as it is the most commonly used acid in acid treatment. The cement is soaked in the HCl solution to determine the acid solubility of these two cements. Different proportions of MOS cement and MOC cement were ground into powder, dried, and then soaked in a 15 mL, 15% HCl solution at 70 °C.[31] After a certain period of time, the remaining cement particles are filtered and dried to a fixed weight; the acid solubility (%) was calculated by the following equation

$$S = \frac{m_1 - m_2}{m_2} \quad (1)$$

where S denotes the acid solubility, %, and m_1 and m_2 are the initial weight of the cement particles and the weight of remaining cement specimen after being dried, respectively, g.

2.6. Plugging Performance of MOC Cement and MOS Cement. The plugging performance of the two kinds of cement was studied using a physical simulation device (Figure 1a). The cement was made into a cylindrical experimental

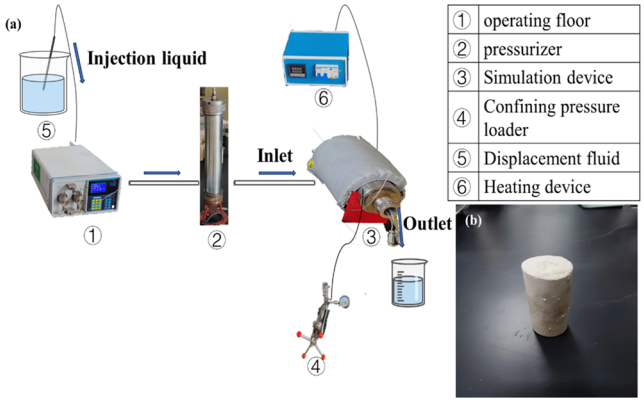

Figure 1. (a) Simulation device for plugging performance of MOS cement and MOC cement. (b) Experimental sample.

sample with a diameter of 25 mm and a height of 50 mm (Figure 1b). The specific test steps of the plugging test were as follows: (a) The prepared sample was put into the simulation device and the temperature of heating device was set to 70 °C. (b) The confining pressure was applied to the sample in the simulation device by using the confining pressure loader to 10 MPa. (c) The pressurizer with an infusion tube was connected to the operating table and the operating table was opened to inject the fluid into the infusion tube until air in the infusion tube is completely discharged. (d) The pressurizer is connected to the simulation device, and the fluid is injected into the simulation device at a rate of 10 mL/min. Moreover, the operating table was also used to record the change in the injection pressure in real time. The maximum pressure corresponds to the pressure bearing capacity of the cement.

2.7. Numerical Simulation Analysis Based on Fluid−Solid Coupling. The Fluent + Transient Structure module of the Workbench simulation platform is used for fluid−solid coupling calculations. In the entire calculation process, the fluid domain first performs several steps to calculate the pressure field distribution and velocity field distribution. These results were then transferred to the structural module for mechanical calculation. The calculation results from the structural module are returned to the flow field for the subsequent calculation. The solution steps are shown in Figure 2. The physical model consists of two main parts: the flow field

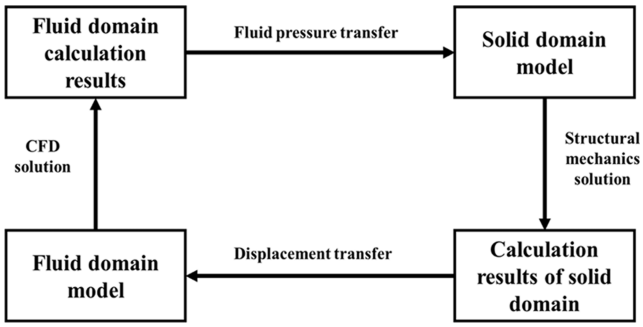

Figure 2. Fluid−solid coupling solution steps.

region and the solid region (Figure 3). The simulation calculation process is realized through three control equations: the fluid control equation, the solid control equation, and the coupling equation (Table 2).

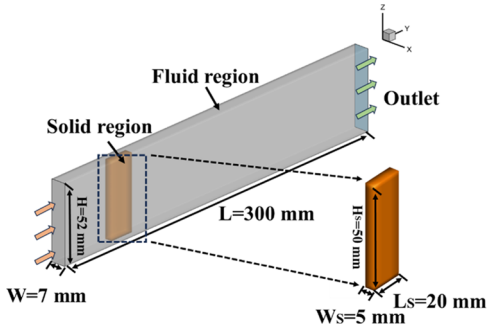

Figure 3. Schematic diagram of the model used in the simulation.

The calculation of the flow field is essentially to solve the physical conservation equations such as the mass equation and the momentum equation. The equation obtained by solving it correctly reflects the change of the flow field.

Table 2. Parameters of the Solid Region

category	compressive strength (MPa)	elastic modulus (N/mm^2)	Poisson ratio
numerical value	23	2.56×10^4	0.23

https://doi.org/10.1021/acsomega.3c07654
ACS Omega 2024, 9, 2696−2706

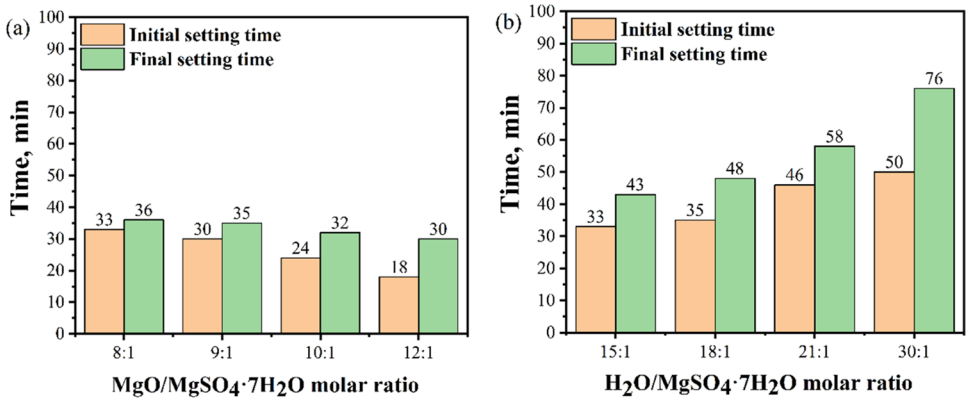

Figure 4. Setting time of MOS cement with different molar ratios of $MgO/MgSO_4{\cdot}7H_2O$ and $H_2O/MgSO_4{\cdot}7H_2O$ at 70 °C: (a) 8−12:1:12 and (b) 10:1:15−21.

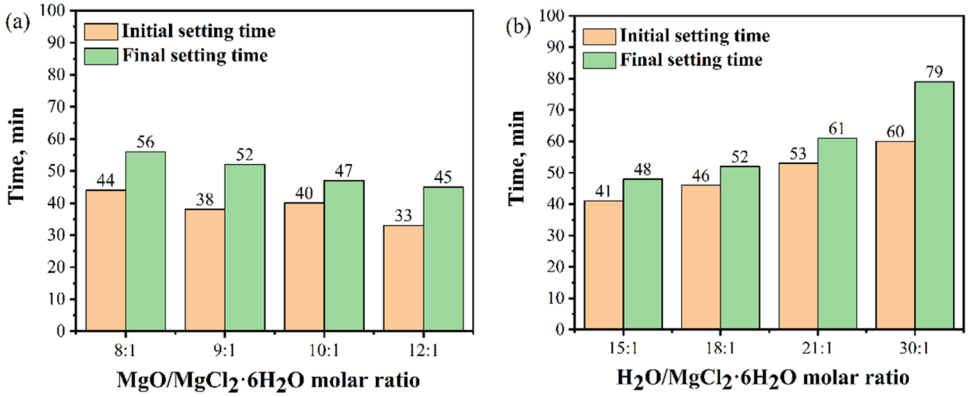

Figure 5. Setting time of MOC cement with different molar ratios of $MgO/MgCl_2{\cdot}6H_2O$ and $H_2O/MgCl_2{\cdot}6H_2O$ at 70 °C: (a) 8−12:1:12 and (b) 10:1:15−21.

$$\frac{\partial \rho}{\partial t} + \frac{\partial(\rho U_i)}{\partial x_i} = 0 \tag{2}$$

$$\frac{\partial(\rho u_i)}{\partial t} = \frac{\partial(\rho u_i u_j)}{\partial x_j} = \rho f_i + \frac{\partial}{\partial x_i}\sigma_{ij} \tag{3}$$

$$\frac{\partial}{\partial t}\left[\left(\frac{1}{2}U^2 + e\right)\right] + \frac{\partial}{\partial x_j}\left[\rho\left(\frac{1}{2}U^2 + e\right)\right]u_j = \rho(f_i u_i + q) + \frac{\partial}{\partial x_j}\left(\sigma_{ij}u_i + \lambda\frac{\partial T}{\partial x_j}\right) \tag{4}$$

where U is the flow velocity in m/s, ρ is the fluid density in kg/m^3, t is the time in seconds, f is the fluid mass force in N, σ_{ij} is the component of the stress tensor, $\frac{1}{2}U^2$ is the internal kinetic energy, e is the internal energy, and q is the calorific value of the fluid given by the heat source.

The solid will vibrate under the influence of a fluid, and its displacement control equation is as follows

$$M_s\frac{d^2r}{dt^2} + C_s\frac{dr}{dt} + K_s r + \tau_s = 0 \tag{5}$$

where M_s is the mass matrix, C_s is the damping matrix, K_s is the stiffness matrix, τ_s is the stress on solids, r is the displacement of the solid, and t is the time.

The fluid−solid coupling contact surface must meet the most basic conservation principles of fluid and solid displacement, flow, temperature, stress, and so on.

$$n{\cdot}\tau_f = n{\cdot}\tau_s \tag{6}$$

$$r_f = r_s \tag{7}$$

$$q_f = q_s \tag{8}$$

$$T_f = T_s \tag{9}$$

where τ is the stress, r is the displacement, q is the calorific value, T is the temperature, f represents the fluid, and s represents the solid.

3. RESULTS AND DISCUSSION

3.1. Setting Time of MOC and MOS Cements. The setting time includes the initial setting time and the final setting time, which are closely related to the changes in the rheological properties of the cement slurry. It is generally necessary to complete the preparation and pumping of the slurry before the initial setting, and the drilling operation can be resumed after final solidification. A suitable initial setting time and a final setting time can ensure that we can pump the plugging slurry into the target area and rapidly form a plugging area. In this way, it is beneficial to shorten the plugging period and reduce costs. The initial and final setting times of MOC and MOS cements are influenced by the ratio of raw materials and temperature.

https://doi.org/10.1021/acsomega.3c07654
ACS Omega 2024, 9, 2696−2706

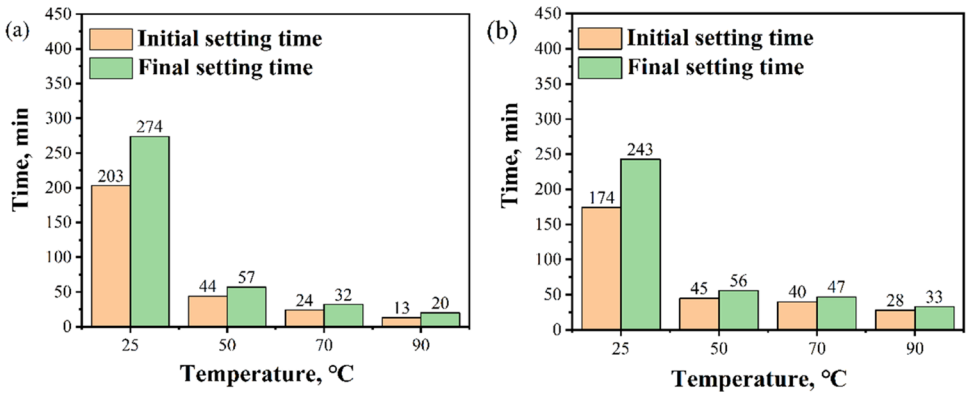

Figure 6. Setting time of MOS cement and MOC cement with molar ratios of 10:1:12 at 25, 50, 70, and 90 °C: (a) MOS cement and (b) MOC cement.

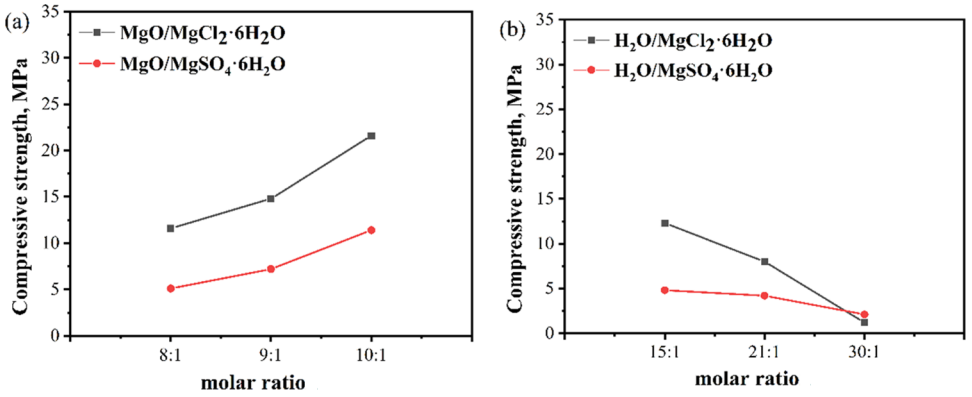

Figure 7. Compressive strength of MOS cement and MOC cement of different molar ratios after curing for 24 h: (a) different MgO additions and (b) different H_2O additions.

3.1.1. Effect of the Raw Material Molar Ratio on the Setting Time of Cement. To determine the effect of the MgO/$MgSO_4{\cdot}7H_2O$ molar ratio and $H_2O/MgSO_4{\cdot}7H_2O$ molar ratio of MOS cement and MgO/$MgCl_2{\cdot}6H_2O$ molar ratio and $H_2O/MgCl_2{\cdot}6H_2O$ molar ratio of MOC cement on the setting time, several slurries of MOS cement and MOC cement with different MgO/$MgSO_4{\cdot}7H_2O$($MgCl_2{\cdot}6H_2O$)/H_2O molar ratios were prepared. Figure 4a illustrates the variation in the setting time of the MOS cement with respect to the MgO/$MgSO_4{\cdot}7H_2O$ molar ratio, which ranges from 8:1 to 12:1. The molar ratio of $H_2O/MgSO_4{\cdot}7H_2O$ was fixed at 12:1. The initial setting time of the slurry is shortened by 45.4%, and the final setting time is shortened by 16.7% when the MgO/$MgSO_4{\cdot}7H_2O$ molar ratio increases from 8 to 12. Figure 4 shows the variation in the setting time of MOS cement based on the $H_2O/MgSO_4{\cdot}7H_2O$ molar ratio, which ranges from 15:1 to 30:1. The MgO/$MgSO_4{\cdot}7H_2O$ ratio was fixed at 12:1. When the molar ratio of $H_2O/MgSO_4{\cdot}7H_2O$ was increased from 15:1 to 30:1, the initial setting time of the slurry was extended by 51% and the final setting time was extended by 16.7%. The data showed that the setting time of the MOS cement is shortened with an increase in the MgO/$MgSO_4{\cdot}7H_2O$ molar ratio. Additionally, the setting time is also shortened with an increase in the $H_2O/MgSO_4{\cdot}7H_2O$ molar ratio. On the other hand, both the initial setting time and final setting time of the cement slurry are prolonged. More MgO particles participate in the hydration reaction, resulting in an increased production of reaction products and an earlier formation of the crystal structure. This leads to an increased curing rate. Furthermore, as the molar ratio of H_2O to $MgSO_4$ increases, the cement slurry becomes more diluted, which leads to a longer setting time.

Figure 5a,b shows the varying molar ratios of MgO/$MgCl_2{\cdot}6H_2O$ and $H_2O/MgCl_2{\cdot}6H_2O$ and their impact on the initial setting time and final setting time of MOC cement. The setting time of MOC cement varies similarly to that of MOS cement. However, MOC cement has a longer setting time compared to MOS cement. The reason for this phenomenon is that the crystallization rate of the MOC cement phase is slow.

3.1.2. Effect of Temperature on Setting. Figure 6a,b shows the variation of the initial setting time and final setting time of MOS and MOC cement slurries at different temperatures (25, 50, 70, and 90 °C) with a MgO/$MgSO_4{\cdot}7H_2O$ ($MgCl_2{\cdot}6H_2O$)/H_2O molar ratio of 10:1:12. At 25 °C, the final setting time of MOC cement is 243 min, while the final setting time of MOS cement is 274 min. When the temperature rises to 50 °C, the setting time decreases significantly. The initial setting time and final setting time of two types of cement decrease as the temperature increases. The rise in temperature accelerates the hydration reaction between the components of cement, leading to the accelerated formation of the crystal structure and a reduced setting time.

It can be seen from Figures 5 and 6 that the appropriate setting time can be obtained by adjusting the molar ratio of the raw materials in MOC cement and MOS cement. The time from the initial setting state to the final setting state of the cement is short. This indicates that when using this cement as

https://doi.org/10.1021/acsomega.3c07654
ACS Omega 2024, 9, 2696−2706

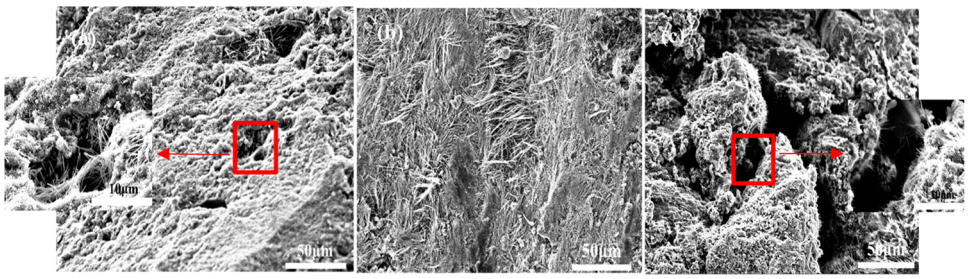

Figure 8. SEM images of MOC cement of different molar ratios of $MgO/MgCl_2{\cdot}6H_2O/H_2O$ after curing at for 24 h: (a) 9:1:12, (b) 10:1:12, and (c) 10:1:21.

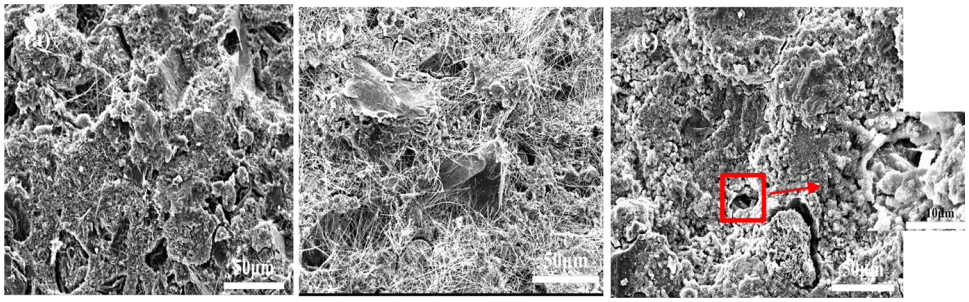

Figure 9. SEM images of MOS cement of different molar ratios of $MgO/MgSO_4{\cdot}7H_2O/H_2O$ after curing for 24 h at (a) 9:1:12, (b) 10:1:12, and (c) 10:1:21.

a plugging material, it can quickly set and form a sealing zone after reaching the loss area.

3.2. Compressive Strength of MOC and MOS Cements. The compressive strength of cement is an important factor when using MOC or MOS cement as a plugging material. High compressive strength of the MOS cement or MOC cement can help improve the load bearing capacity of the weak zone. The compressive strength of these two types of cement depends on the microstructure, which is significantly influenced by the proportion of raw materials.[32,33]

3.2.1. Effect of the Raw Material Molar Ratio on the Compressive Strength of MOS and MOC Cements. Figure 7 shows the strength variation of MOC and MOS cements under different molar ratios of raw materials, and the strength change patterns of the two types of cements are similar. With an increase in the MgO content, the strength of the cement also increases. However, the strength of both types of cements decreases as the H_2O content increases. These findings indicate that a higher compressive strength can be achieved by increasing the MgO content or reducing the H_2O content in cement. In addition, it can be observed from Figure 7 that the compressive strength of the MOS cement is lower than that of the MOC cement. This difference can be attributed to the low solubility of $MgSO_4$ in water.

3.2.2. Microstructure of MOC Cement and MOS Cement. The above-mentioned MOS and MOC cement strengths are affected by the microstructure. Better crystal growth and a more compact structure could result in higher physical strength.[34,35] SEM images of MOC cement exhibiting different molar ratios of $MgO/MgCl_2{\cdot}6H_2O/H_2O$ are illustrated in Figure 8. The structure of the MOS becomes more compact and denser when the molar ratio of MgO to $MgCl_2{\cdot}6H_2O$ increases from 9:1 to 10:1, while the molar ratio of H_2O to $MgCl_2{\cdot}6H_2O$ remains fixed at 12:1. This phenomenon occurs because residual MgO (either due to low reactivity or an excess amount) can act as a filler and improve the compactness. As the molar ratio of $H_2O/MgCl_2{\cdot}6H_2O$ increases from 12:1 to 21:1, with the $MgO/MgCl_2{\cdot}6H_2O$ molar ratio fixed at 10:1, the crystal phases become incomplete (Figure 6c). The reason for this phenomenon is that an increase in water leads to an enlargement of the gap between the hydration products, which reduces their connectivity and compactness. Therefore, the compressive strength will change, depending on the molar ratio of raw materials.

Figure 9 illustrates the variation at different $MgO/MgSO_4{\cdot}7H_2O/H_2O$ molar ratios of the MOS cement. The voids of MOS cement are filled with an excessive amount of MgO, resulting in a denser overall structure. This increase in the $MgO/MgSO_4{\cdot}7H_2O$ molar ratio contributes to the densification. As the molar ratio of $H_2O/MgSO_4{\cdot}7H_2O$ increases from 12:1 to 21:1, with the $MgO/MgSO_4{\cdot}7H_2O$ molar ratio fixed at 10:1, the increase in the H_2O content leads to a decrease in the $MgSO_4$ concentration. This, in turn, causes the gap between the hydration products to expand.[35] From a microperspective, compared with MOC cement (Figure 6b), the surface connectivity of MOS cement is not complete (Figure 9b), so the compressive strength of MOS cement is lower than that of MOC cement.

Due to the presence of natural fractures, conventional plugging materials are unable to effectively withstand wellbore fluid erosion and formation fluid erosion. Therefore, the plugging layer is easily diluted and washed away, resulting in repeated losses. MOS or MOC cement is injected into the well as a plugging agent, which is not limited by the shape or size of the crack. The cement reaches the target area before it reaches the initial setting state. The downhole temperature catalyzes the formation of the main strength phase of the cement, allowing it to quickly form a plugging layer with a certain strength. Thus, the pressure bearing capacity of the leakage zone is improved, and further expansion of the crack is prevented.

https://doi.org/10.1021/acsomega.3c07654
ACS Omega 2024, 9, 2696−2706

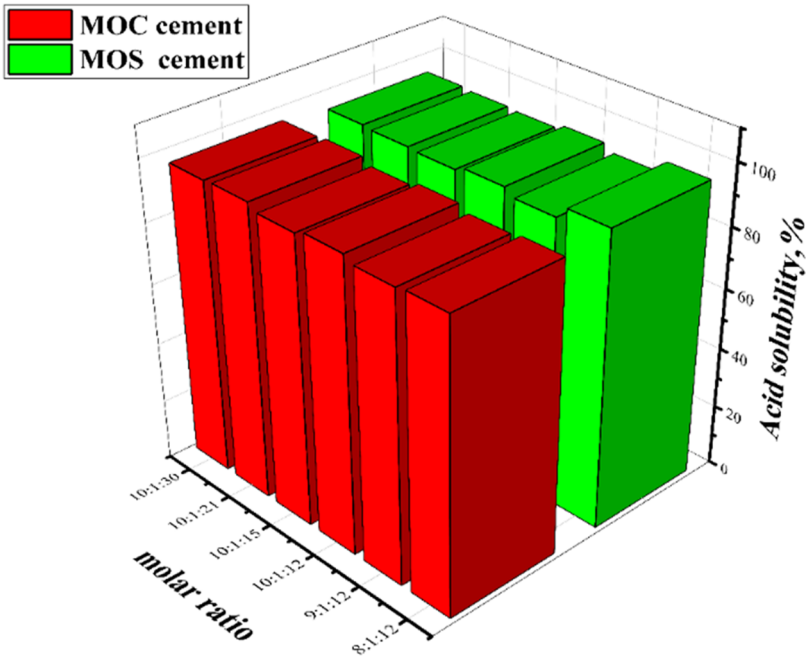

Figure 10. Acid solubility of MOS cement and MOC cement of different molar ratios in 15% HCl solutions for 120 min.

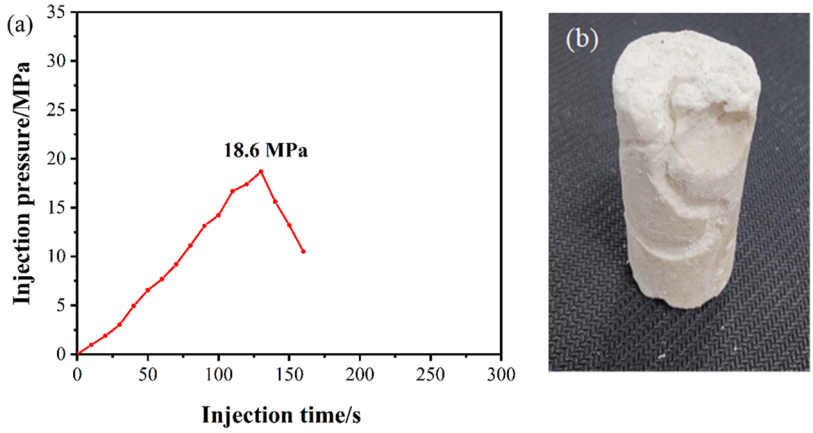

Figure 11. Plugging performance of MOS cement with $MgO/MgSO_4{\cdot}7H_2O/H_2O$ molar ratios of 10:1:12: (a) pressure bearing capacity of MOS cement and (b) damaged cement.

3.3. Acid Solubility. The commonly used G-type cement generally exhibits a low acid solubility because the siliceous component forms a protective coating around the cement, preventing further dissolution. The solubility of class G cement can be improved by adding acid-soluble components such as $CaCO_3$. The solubility was 9.3% without the presence of $CaCO_3$ and 52.0% with the presence of 200% $CaCO_3$ by weight of cement in 15% HCl after 120 min.[30,36] Acid-soluble fibers and certain rigid acid-soluble particles are frequently employed as temporary plugging materials. However, their acid solubility is relatively low, at approximately 70%.[37] Compared with the acid-soluble materials mentioned above, MOS cement and MOC cement exhibit significantly higher acid solubility and a faster dissolution rate. Figure 10 shows the solubility of MOC and MOS cement with different ratios after soaking in 15% hydrochloric acid solution at 70 °C for 120 min. It can be seen from the data that the acid solubilities of different ratios are almost the same, and all are about 95%. $5Mg(OH)_2{\cdot}MgCl_2{\cdot}8H_2O$, $3Mg(OH)_2{\cdot}MgCl_2{\cdot}8H_2O$, $Mg(OH)_2$, and other main hydration products of MOC cement will disintegrate on exposure to acid due to leaching of $MgCl_2$. The dissolution of MOS cement in HCl solution is due to reactions of the acid with Mg $(OH)_2$ and the 5-1-2 phase. The reactions between MOS cement and HCl are expressed as follows

$$Mg(OH)2(s) + 2HCl(aq) \rightarrow MgCl_2(aq) + 2H_2O$$

$$5Mg(OH)_2{\cdot}MgSO_4{\cdot}2H_2O(s) + 10HCl(aq) \rightarrow 5MgCl_2(aq) + MgSO_4(aq) + 12H_2O$$

After completing the drilling operation, the cement undergoes acid treatment, which gradually leaches out the ions in the cement. This process leads to decomposition of the cementing phase. This process accelerates the dissolution of the cement, allowing for the rapid restoration of permeability.

3.4. Plugging Performance of MOC Cement and MOS Cement. MOS cement slurry with $MgO/MgSO_4{\cdot}7H_2O/H_2O$ molar ratios of 10:1:12 and 10:1:21 and MOC cement slurry with the same molar ratio of $MgO/MgCl_2{\cdot}6H_2O/H_2O$ were

https://doi.org/10.1021/acsomega.3c07654
ACS Omega 2024, 9, 2696−2706

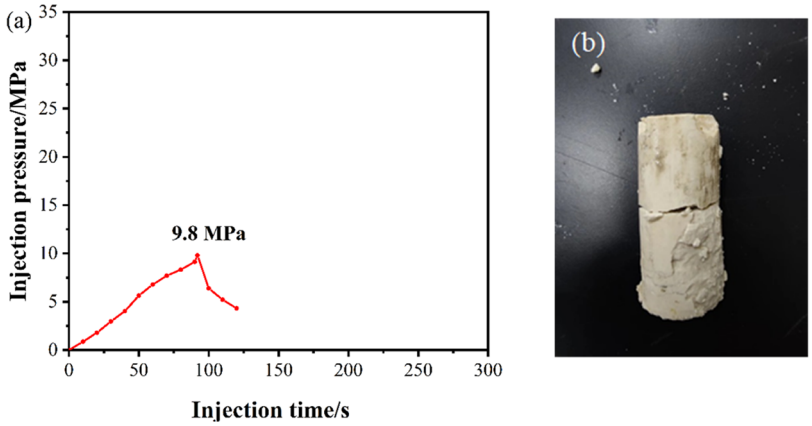

Figure 12. Plugging performance of MOS cement with $MgO/MgSO_4{\cdot}7H_2O/H_2O$ molar ratios of 10:1:21: (a) pressure bearing capacity of MOS cement and (b) damaged cement.

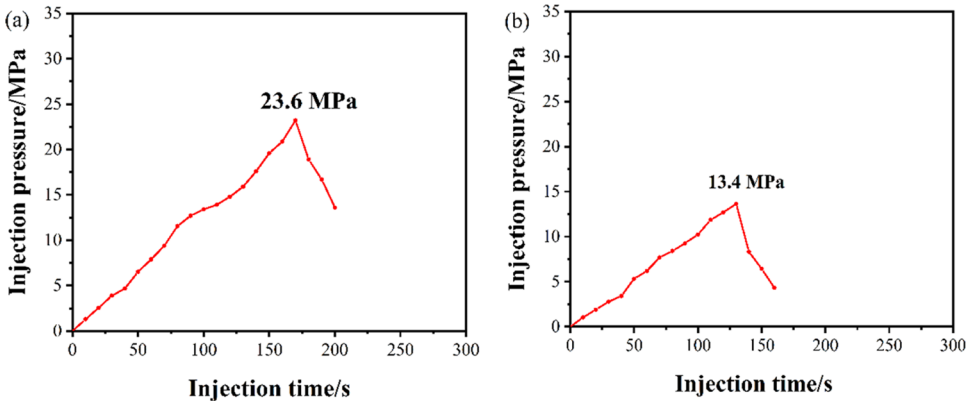

Figure 13. Plugging performance of MOC cement with different $MgO/MgCl_2{\cdot}6H_2O/H_2O$ molar ratios: (a) 10:1:12 and (b) 10:1:21.

prepared as plugging slurries. MOS cement and MOC cement exhibit higher compressive strength at a molar ratio of 10:1:12, while both cements demonstrate lower strength at a molar ratio of 10:1:21. By testing the plugging performance of the aforementioned cements with varying strengths, it is possible to comprehensively evaluate the pressure bearing capacity of MOS cement and MOC cement.

3.4.1. MOS Plugging Slurry. The experiment on the sealing pressure bearing capacity of cement is shown in Figure 11a. When the pressure bearing capacity of the cement reaches 18.6 MPa, there is an instantaneous decrease in pressure. This phenomenon occurs because the column has been damaged by fluid pressure, causing a reduction in the pressure bearing capacity of the cement and allowing the displacement fluid to gradually flow out of the damaged area. Figure 11b shows the change of the MOS cement sample with a $MgO/MgSO_4{\cdot}7H_2O/H_2O$ molar ratio of 10:1:12 after the plugging experiment. It can be observed that the cement sample is mostly intact, although the water blocking end is slightly damaged. Additionally, there are grooves on the cylinder surface that have been eroded by the fluid.

As shown in Figure 12a, the maximum pressure of the MOS cement plugging slurry under this ratio is 9.8 MPa. Figure 12b shows the change of the MOS cement sample with a $MgO/MgSO_4{\cdot}7H_2O/H2O$ molar ratio of 10:1:21 after the plugging experiment. It can be seen that the cylinder was broken in the middle. Compared to MOS cement with a molar ratio of 10:1:12, its pressure bearing capacity is significantly reduced and the degree of damage to the sample is more severe. The loose crystal structure leads to a decrease in its pressure bearing capacity. However, it still demonstrates good performance in the plugging test.

3.4.2. MOC Plugging Slurry. Figure 13a,b shows the sealing and pressure bearing performance of MOC cement slurry with $MgO/MgCl_2{\cdot}6H_2O/H_2O$ molar ratios of 10:1:12 and 10:1:21, respectively. The maximum bearing capacity of the two is 23.6 and 13.4 MPa, respectively. The microstructure of MOC cement is more compact, and it has a high level of crystal continuity, which enhances its plugging effect.

3.5. Fluid−Solid Coupling Analysis. In the flow field, the presence of a solid object will cause changes in the pressure field within the fluid domain, and the movement of the fluid will also affect the solid. The analysis time is set to 10 s, and the time step is 0.01 s. The simulation involves studying the pressure changes in the flow field at various flow rates as well as analyzing the stress distribution and deformation of the cement solid when subjected to fluid forces.

3.5.1. Analysis of the Fluid Region. Figure 14 shows the pressure distribution of the flow field at the middle section under various flow velocities. As the flow rate increases, the pressure of the flow field also gradually increases. When the flow rate is 5 m/s, the pressure at the maximum water pressure is only 0.05 MPa, and there is almost no pressure at the outlet end. However, the maximum water pressure in the flow field reaches 0.16 MPa when the flow rate increases to 10 m/s. Additionally, it can be seen from the diagram that the fluid pressure is concentrated on one side of the solid domain, and the pressure at the outlet end is very low. This phenomenon

https://doi.org/10.1021/acsomega.3c07654
ACS Omega 2024, 9, 2696−2706

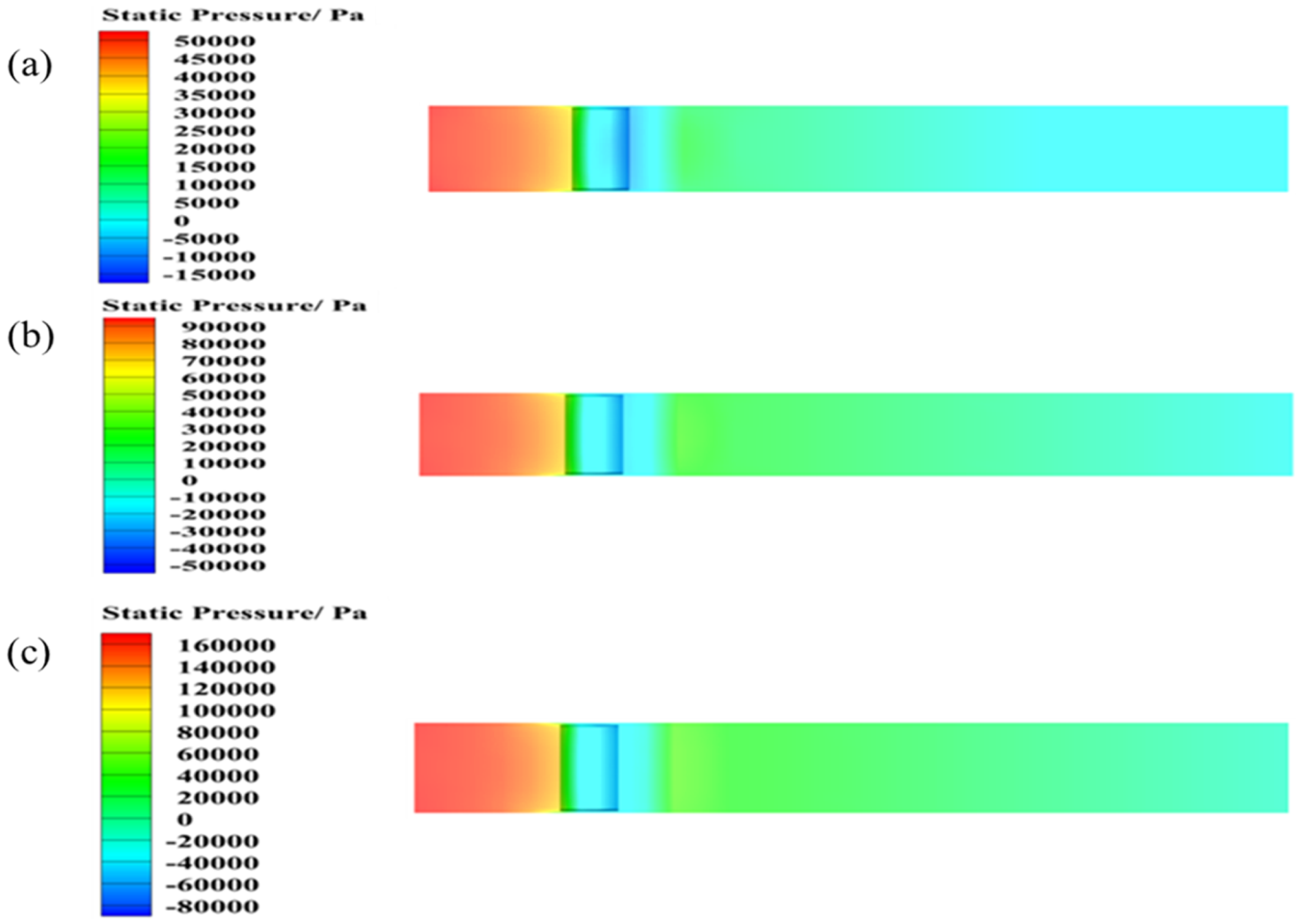

Figure 14. Flow field pressure diagram of different flow velocities: (a) 5 m/s; (b)7.5 m/s; and (c)10 m/s.

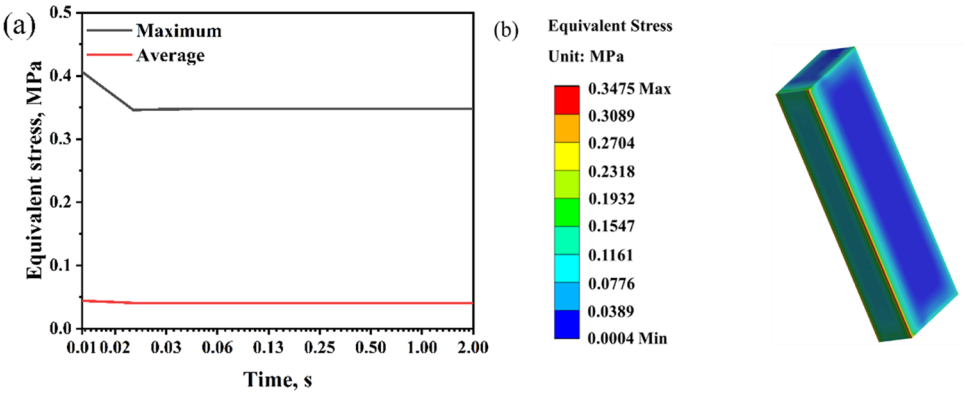

Figure 15. (a) Equivalent stress change diagram in 2 s. (b) Equivalent stress distribution diagram.

occurs because the presence of the solid domain obstructs the fluid flow, causing most of the fluid to be trapped on the left side of the solid domain.

3.5.2. Analysis of the Solid Region. Figure 15a shows the change in the maximum equivalent stress and average equivalent stress of the solid within 2 s at a flow rate of 10 m/s. Under the action of the fluid, the average equivalent stress is small and does not fluctuate too much. This indicates that the solid is less affected by the flow. At 0.01 s, the maximum stress value of the solid is 0.4 MPa, and the subsequent maximum stress value gradually decreases and stabilizes at 0.3 MPa. When the fluid come into contact with the solid, the stress on the solid will increase sharply due to the impact force. After the fluid stabilizes, the stress value of the solid will also decrease and stabilize. Under the action of the fluid, stress is primarily concentrated in the corner area at the front of the solid (Figure 15b), with only a minimal amount of stress being transmitted to the middle and rear of the solid. This indicates that the edge region of the solid is more susceptible to destruction, while the middle and rear parts are less impacted. To further investigate the force exerted on the solid during fluid impact, the time step is adjusted to 0.0001 s and the calculation time is set to 0.05 s. It can be seen from Figure 16 that the maximum equivalent stress at the edge of the solid

https://doi.org/10.1021/acsomega.3c07654
ACS Omega 2024, 9, 2696−2706

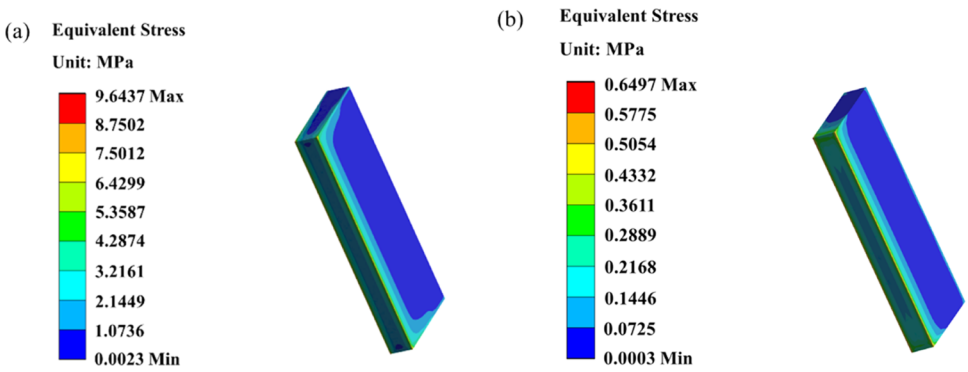

Figure 16. Equivalent stress distribution at different times: (a) 0.0001 s and (b)0.05 s.

reaches 9.6 MPa during fluid impact and remains stable at 0.65 MPa at 0.05 s. Based on the strength data of cement, it can be concluded that the solid remains intact without significant damage under the impact of the fluid.

4. CONCLUSIONS

In the present study, MOC cement and MOS cement were developed as lost circulation materials to address losses that occur during geothermal drilling. The setting time, compressive strength, acid solubility, and plugging ability of MOC and MOS cements with different molar ratios were tested using various test methods. Given the results, the following conclusions are drawn:

(1) The setting time of MOC cement and MOS cement decreases, with the rise of temperature. Increasing the amount of MgO or reducing the amount of H_2O can prepare cement with a shorter setting time.

(2) A higher molar ratio of $MgO/MgSO_4{\cdot}7H_2O$($MgCl_2{\cdot}6H_2O$) and lower molar ratio of $H_2O/MgSO_4{\cdot}7H_2O$-($MgCl_2{\cdot}6H_2O$) are conducive to high compressive strength.

(3) After immersing the MOC cement and MOS cement in a 15% HCl solution for 120 min, the acid solubility was found to be above 95%. This indicates that the acid treatment was successful in removing cement and effectively restoring the permeability of the production zone.

(4) MOC cement and MOS cement show excellent plugging and pressure bearing capacity. Their maximum bearing capacity can reach 18.7 and 23.6 MPa, respectively.

(5) Temporary plugging cement can effectively prevent the flow of a high-speed fluid. Under the action of the fluid, the stress in the cement is primarily distributed at the front and edge area.

(6) The raw materials for synthesizing temporary plugging agents have been industrialized, resulting in low cost. Therefore, MOS cement and MOC cement can be used in industrial applications, particularly in the field of geothermal temporary plugging.

AUTHOR INFORMATION

Corresponding Author

Yuxiu An − *School of Engineering and Technology, China University of Geosciences (Beijing), Beijing 100083, China;* orcid.org/0000-0002-3156-0655; Email: anyx@cugb.edu.cn, 13522045597@163.com

Authors

Liangliang Yan − *School of Engineering and Technology, China University of Geosciences (Beijing), Beijing 100083, China*

Shaocong Pang − *School of Engineering and Technology, China University of Geosciences (Beijing), Beijing 100083, China; Zhengzhou Institute, China University of Geosciences (Beijing), Zhengzhou, Henan 450001, China;* orcid.org/0000-0003-2879-4829

Haiyan Dong − *No. 1 Exploration Institute of Geology and Mineral Resources of Shandong Province, Jinan 250109, China*

Xiuhua Zheng − *School of Engineering and Technology, China University of Geosciences (Beijing), Beijing 100083, China;* orcid.org/0000-0002-3034-0407

Complete contact information is available at: https://pubs.acs.org/10.1021/acsomega.3c07654

Notes

The authors declare no competing financial interest.

ACKNOWLEDGMENTS

The authors would like to acknowledge the financial support of the Science and Technology Innovation Special Project of Xiong'an New Area (2022XAGG0500) for this work.

REFERENCES

(1) Song, X.; Li, G.; Huang, Z.; Shi, Y.; Wang, G.; Song, G.; Xu, F. Review of high-temperature geothermal drilling and exploitation technologies. *Gondwana Res.* **2023**, *122*, 315.

(2) Allahvirdizadeh, P. A review on geothermal wells: Well integrity issues. *J. Cleaner Prod.* **2020**, *275*, No. 124009.

(3) Vivas, C.; Salehi, S. Rheological investigation of effect of high temperature on geothermal drilling fluids additives and lost circulation materials. *Geothermics* **2021**, *96*, No. 102219.

(4) Lukawski, M. Z.; Anderson, B. J.; Augustine, C.; Capuano, L. E.; Beckers, K. F.; Livesay, B.; Tester, J. W. Cost analysis of oil, gas, and geothermal well drilling. *J. Pet. Sci. Eng.* **2014**, *118*, 1−14.

(5) Magzoub, M.; Anyaezu, T.; Salehi, S.; Li, G.; Fan, J.; Teodoriu, C.; Saleh, F. K.; Taleghani, A. D. Evaluating sealability of blended smart polymer and fiber additive for geothermal drilling with the effect of fracture opening size. *J. Pet. Sci. Eng.* **2021**, *206*, No. 108998.

(6) Elkatatny, S.; Ahmed, A.; Abughaban, M.; Patil, S. Deep Illustration for Loss of Circulation While Drilling. *Arab. J. Sci. Eng.* **2020**, *45* (2), 483−499.

(7) Xu, C.; Zhang, H.; She, J.; Jiang, G.; Peng, C.; You, Z. Experimental study on fracture plugging effect of irregular-shaped lost circulation materials. *Energy* **2023**, *276*, No. 127544.

(8) Kandari, M.; Yulianto, G.; Saptadi, S. Analysis of risk factors nonproductive time on geothermal drilling in Indonesia. *AIP Conf. Proc.* **2020**, *2217* (1), No. 030113, DOI: 10.1063/5.0000918.
(9) Xu, C.; Zhang, H.; Kang, Y.; Zhang, J.; Bai, Y.; Zhang, J.; You, Z. Physical plugging of lost circulation fractures at microscopic level. *Fuel* **2022**, *317*, No. 123477.
(10) Chellappah, K.; Aston, M.; Maltby, T.; Savari, S.; Whitfill, D. L. In *Engineered Nutshell Particles for Wellbore Strengthening*, IADC/SPE Drilling Conference and Exhibition, 2018; D021S011R006, Vol. Day 2 Wed, March 07, 2018.
(11) Isaac Prince, E.; Dosunmu, A.; Anyanwu, C. In *Laboratory Study of Oil Palm Kernel Shells and Mangrove Plant Fiber Banana Trunk Fiber as Lost Circulation Materials in Synthetic Based Drilling Mud*, SPE Nigeria Annual International Conference and Exhibition, 2019; D033S027R007, Vol. Day 3 Wed, August 07, 2019.
(12) Kaageson-Loe, N.; Sanders, M. W.; Growcock, F.; Taugbøl, K.; Horsrud, P.; Singelstad, A. V.; Omland, T. H. In *Particulate-Based Loss-Prevention Material - The Secrets of Fracture Sealing Revealed!*, IADC/SPE Drilling Conference, 2008; SPE-112595-MS, Vol. All Days, 2008.
(13) Bybee, K. Large-Volume Cement Squeezes for Severe-Loss Zones. *J. Pet. Technol.* **2010**, *62* (05), 82−85.
(14) Alsaba, M.; Nygaard, R.; Saasen, A.; Nes, O.-M. *Laboratory Evaluation of Sealing Wide Fractures Using Conventional Lost Circulation Materials*, SPE Annual Technical Conference and Exhibition, 2014; SPE-170576-MS, Vol. All Days, 2014.
(15) Kumar, A.; Savari, S.; Whitfill, D. L.; Jamison, D. E. In *Wellbore Strengthening: The Less-Studied Properties of Lost-Circulation Materials*, SPE Annual Technical Conference and Exhibition, 2010; SPE-133484-MS, Vol. All Days, 2010.
(16) Nasiri, A.; Ghaffarkhah, A.; Dijvejin, Z. A.; Mostofi, M.; Moraveji, M. K. Bridging performance of new eco-friendly lost circulation materials. *Pet. Explor. Dev.* **2018**, *45* (6), 1154−1165.
(17) Razavi, O.; Vajargah, A. K.; van Oort, E.; Aldin, M. Comprehensive analysis of initiation and propagation pressures in drilling induced fractures. *J. Pet. Sci. Eng.* **2017**, *149*, 228−243.
(18) Sweatman, R. E.; Scoggins, W. C. Acid-Soluble Magnesia Cement: New Applications in Completion and Workover Operations. *SPE Prod. Eng.* **1990**, *5* (04), 441−447.
(19) Magzoub, M. I.; Salehi, S.; Hussein, I. A.; Nasser, M. S. Loss circulation in drilling and well construction: The significance of applications of crosslinked polymers in wellbore strengthening: A review. *J. Pet. Sci. Eng.* **2020**, *185*, No. 106653.
(20) Pan, Y.; Cui, X.; Wang, H.; Lou, X.; Yang, S.; Oluwabusuyi, F. F. Research Progress of Intelligent Polymer Plugging Materials. *Molecules* **2023**, *28* (7), No. 2975, DOI: 10.3390/molecules28072975.
(21) Ashena, R.; Ghalambor, A.; Elmgerbi, A.; Hekmatinia, A.-A.; Mubashir, M. Level-off cement plugging method to cure lost circulation verified with case studies. *J. Pet. Explor. Prod. Technol.* **2021**, *11* (6), 2777−2789.
(22) Tan, H.; Shen, L.; Zuo, Y.; Fan, L.; Zhang, G.; Qiu, D.; Xie, L.; Zheng, X.; He, W. Light-weight temporary-sealing cement for medium temperature geothermal wells by using polyvinyl alcohol fibers and fly ash Cenospheres. *J. Pet. Sci. Eng.* **2022**, *215*, No. 110704.
(23) Vinson, E. F.; Totten, P. L.; Middaugh, R. L. In *Acid Removable Cement System Helps Lost Circulation in Productive Zones*, IADC/SPE Drilling Conference, 1992; SPE-23929-MS, Vol. All Days, 1992.
(24) Mata, F.; Veiga, M. In *Crosslinked Cements Solve Lost Circulation Problems*, SPE Annual Technical Conference and Exhibition, 2004; SPE-90496-MS, Vol. All Days, 2004.
(25) Li, Z.-g.; Ji, Z.-s. Effect of Molar Ratios on Compressive Strength of Modified Magnesium Oxysulfate Cement. *Int. J. Hybrid Inf. Technol.* **2015**, *8* (6), 87−94.
(26) Walling, S. A.; Provis, J. L. Magnesia-Based Cements: A Journey of 150 Years, and Cements for the Future? *Chem. Rev.* **2016**, *116* (7), 4170−4204.
(27) Qin, L.; Gao, X.; Li, W.; Ye, H. Modification of Magnesium Oxysulfate Cement by Incorporating Weak Acids. *J. Mater. Civ. Eng.* **2018**, *30* (9), No. 04018209.
(28) Zeng, X.; Yu, H.; Wu, C. An Overview of Study on Basic Magnesium Sulfate Cement and Concrete in China (2012−2019). *KSCE J. Civ. Eng.* **2019**, *23* (10), 4445−4453.
(29) Cui, K.-X.; Jiang, G.-C.; Yang, L.-L.; Deng, Z.-Q.; Zhou, L. Preparation and properties of magnesium oxysulfate cement and its application as lost circulation materials. *Pet. Sci.* **2021**, *18* (5), 1492−1506.
(30) Luke, K.; Soucy, K. In *Test Method to Optimize Acid-Soluble Cement for Unconventional Gas Completions*, CIPC/SPE Gas Technology Symposium 2008 Joint Conference, 2008; SPE-114759-MS, Vol. All Days, 2008.
(31) Jadhav, R.; Patil, S. In *Acid-Soluble Thixotropic Cement System for Lost Circulation Challenges*, Abu Dhabi International Petroleum Exhibition & Conference, 2018; D022S135R002, Vol. Day 2 Tuesday, November 13, 2018.
(32) Seymour, B.; Santra, A. In *Detailed Laboratory Investigation of Acid Soluble Cements as Solution for Lost Circulation Across the Producing Zones*, SPE/IADC Middle East Drilling Technology Conference & Exhibition, 2013; SPE-166804-MS, Vol. All Days, 2013.
(33) Suyan, K. M.; Sharma, V.; Jain, V. K. In *An Innovative Material for Severe Lost Circulation Control in Depleted Formations*, Middle East Drilling Technology Conference & Exhibition, 2009; SPE-125693-MS, Vol. All Days, 2009.
(34) Fu, J.-g.; Liang, W.; Wang, H.; He, Z.-x. Synthesis and characterization of MgSO4·5Mg(OH)2·2H2O flake powders. *J. Cent. South Univ. Technol.* **2011**, *18* (6), 1871−1876.
(35) Li, J.; Xiang, L.; Jin, Y. Hydrothermal formation of magnesium oxysulfate whiskers in the presence of ethylenediaminetetraacetic acid. *J. Mater. Sci.* **2006**, *41* (5), 1345−1348.
(36) Miranda, C. R.; Gold, J. S. In *Study of Cement Resistance to the Attack of Acid Solutions*, International Symposium on Oilfield Chemistry, 1997.
(37) van Oort, E.; Friedheim, J.; Pierce, T.; Lee, J. Avoiding Losses in Depleted and Weak Zones by Constantly Strengthening Wellbores. *SPE Drill. Completion* **2011**, *26* (04), 519−530.

https://doi.org/10.1021/acsomega.3c07654
ACS Omega 2024, 9, 2696−2706